## PAPER

Check for updates

# Understanding nucleation efficiency of stereocomplex-crystallites on homochiral crystallization in poly(L-lactide)/poly(D-lactide) blends: homogenization near crystal growth front

Qi Chen, [a,b] Mansurali Mithani,[a] Rafael Auras, [c] Jacob Judas Kain Kirkensgaard [d,e] and Ilke Uysal-Unalan *[a,b]

Understanding the concurrent behavior of homochiral (HC) and stereocomplex (SC) crystallization in stereocomplex polylactide (SCPLA) is crucial for developing polymorphic SCPLA-based materials for a range of applications. This work explores the SC-nucleated HC crystallization behavior in symmetric, poly (ethylene glycol)-plasticized, and asymmetric SCPLA systems under both non-isothermal and isothermal conditions. Pre-existing SC crystals with different states were generated by annealing samples at various temperatures, and their influence was assessed through nucleation efficiency (NE), Avrami exponents, and the crystallization half-time of SC-nucleated HC crystallization. Variations in the results can be attributed to differences in the concentration of $10_3$ helices in local regions near the crystal growth front following SC crystallization. This work suggests that a dynamic equilibrium between thermal fluctuation, composition gradient-driven homogenization, and nucleation-driven aggregation processes control the concentration of these helices. Aggregation enriches local regions with $10_3$ and $3_1$ helices, promoting both HC and SC nucleation while restricting random-coil diffusion, whereas homogenization disperses these ordered segments into the surrounding matrix, diminishing their local influence. This mechanistic perspective offers new insight into the interplay between helical accumulation and matrix relaxation in SC-nucleated HC crystallization and provides guidance for the design of next-generation polymorphic SCPLA-based materials.

[a]*Department of Food Science, Aarhus University, Agro Food Park 48, 8200 Aarhus N, Denmark. E-mail: iuu@food.au.dk*
[b]*CiFOOD – Center for Innovative Food Research, Aarhus University, Agro Food Park, 48, 8200 Aarhus N, Denmark*
[c]*School of Packaging, Michigan State University, East Lansing, MI 48824-1223, USA*
[d]*Department of Food Science, University of Copenhagen, 1958 Frederiksberg C, Denmark*
[e]*Niels Bohr Institute, University of Copenhagen, 2100 Copenhagen Ø, Denmark*

## Introduction

The emerging interest in stereocomplex polylactide (SCPLA), derived from a poly(L-lactide) (PLLA) and poly(D-lactide) (PDLA) mixture, arises from its potential to enhance the properties of PLA-based materials.[1–3] The SC-crystal fraction in SCPLA is crucial in exploiting its advantageous properties, such as a higher melting temperature than homochiral crystals.[4] Obtaining a substantial SC-crystal fraction in high-molecular-weight SCPLA presents a challenge initially linked to the diffusion barrier associated with cooperative racemate pairing and folding. Further research highlighted other challenging factors, such as phase separation[5,6] and nucleation mode,[7] in

determining the crystallization of SC and HC. Several strategies, such as plasticizer addition[8] and selective nucleators,[9] have successfully promoted selective SC-crystallization,[8–11] despite an incomplete understanding of the underlying mechanisms. Particularly, the promotion of racemate pairing *via* applying a shear field or nucleating agent can facilitate optimal SC-crystallization conditions.[9,12] However, the suppressed HC-crystallization behavior in the meantime, despite the clear nucleation effect of SC-crystals on HC crystallization, remains elusive. A thorough comprehension of HC crystallization behavior in the context of SC crystallization is critical to understanding the competition between HC and SC crystallization.

Alongside the spontaneous suppression of HC crystallization in the systems favoring SC crystallization, diverse HC crystallization behaviors can be witnessed in SC-nucleated HC crystallization experiments.[13–25] The nucleation efficiency (NE) of SC-nucleated HC crystallization is found to be dependent on the ratio of PLLA to PDLA, with near-equivalent composition leading to the formation of more heterogeneous nucleation sites and an elevated NE.[15] Researchers have sought to explore this nucleation effect. Narita *et al.*[18,20,21] investigated

© 2026 The Author(s). Published by the Royal Society of Chemistry

*RSC Appl. Polym.*, 2026, **4**, 651–661 | **651**

the temperature correlation and the intricate relationship between NE and structural parameters of pre-existing SC-crystals formed from different PLLA/PDLA ratios and molecular weights. Various approaches have been undertaken to elucidate this mechanism. Wen *et al.*[26] dismissed the lattice matching type epitaxy mechanism by crystallographic characterization, while Wang *et al.*[27] emphasized the role of the interfacial free energy difference between foreign surfaces and PLLA crystals when comparing the nucleation of PLLA by different fibers, including SCPLA fiber. Some studies have also considered the influence of the SC-crystal network structure. For instance, Rahman *et al.*[24] proposed that local stress could be built up within the SC-crystal network, triggering stress-induced nucleation of HC crystallization. On the other hand, Lv *et al.*[25] suggested that the SC-crystal network might prolong the retention time of HC-crystal memory. Despite many research efforts, the mechanism driving NE variation in SC-nucleated HC crystallization remains an area of continued investigation and puzzle.

A clear understanding of SC-nucleated HC crystallization behavior requires consideration of the independence between nucleation and crystal growth. Wei *et al.*[19] noted the simultaneous promotion of HC nucleation and suppression of overall HC crystallization within the SC-crystal network. During the nucleation or early stage of crystallization, before the chain attaches to the nuclei, it has been suggested that PLA chains adopt a state of local ordering[28] near the crystal growth front to minimize the free energy pathway, adhering to the Ostwald rule.[29,30] Concerning this, our prior work proposed frozen local ordering near the growth front, which leads to an increase in the rigid amorphous fraction.[9] Other researchers have proposed various theories regarding the early stage of SC crystallization, such as the transformation of $10_3$ (as a precursor for HC crystallization) to $3_1$ helices (as a precursor for SC crystallization) driven by hydrogen bonding interaction between enantiomers,[31] and the accumulation of unmatched PLLA or PDLA acting as impurities for SC crystallization.[32] To comprehend the underlying mechanisms of SC-nucleated HC crystallization and its intricate behavior, this study utilized self-nucleation experiments to induce various states of SC-crystals at different temperatures. The chain states in the early crystallization stage were considered with the aid of poly(ethylene glycol), PEG, addition, and asymmetric composition. The isothermal HC crystallization under different states of SC-crystal formed at different temperatures was analyzed by the Avrami equation to unravel the behavior.

## Experimental section

### Raw materials

PLLA (trade name Luminy® L130 with $M_w$ *ca.* 160 kg mol$^{-1}$, D-lactide content <1%) and PDLA pellets (trade name Luminy® D120 with $M_w$ *ca.* 120 kg mol$^{-1}$, L-lactide content <1%) were purchased from TotalEnergies Corbion (Gorinchem, Netherlands). The PEG (trade name PEG600) and dichloromethane (DCM) were purchased from Sigma-Aldrich (Søborg, Denmark).

### Preparation of stereocomplex PLA

The SCPLA blends were prepared through the solvent casting method. Equal amounts of PLLA and PDLA pellets were dissolved in DCM at a concentration of 5 wt% under magnetic stirring overnight at room temperature. The resulting solution was poured into a glass Petri dish and left to dry at ambient conditions overnight. Afterward, the films were dried in an oven at 70 °C for 12 hours to ensure complete solvent evaporation. These films were designated as SCPLA films. For the preparation of plasticized SCPLA blends, PEG was added at a concentration of 2 wt% relative to the dry weight of SCPLA. The PEG was mixed with the PLLA/PDLA solution under magnetic stirring, followed by the same solvent casting procedure described above. The resulting films were denoted as PEG2. To create asymmetric SCPLA blends, a ratio of 90 : 10 of PLLA to PDLA was mixed and dissolved in a 5 wt% DCM solution. The solvent casting procedure was then carried out following the abovementioned steps. The resulting films obtained were named L90.

### Differential scanning calorimetry

The SC-nucleated HC crystallization of the solvent-casted films was investigated using differential scanning calorimetry (DSC) (Q2000, TA instruments, New Castle, USA) equipped with an RCS 90 cooler, operated under a nitrogen gas flow of 50 mL min$^{-1}$. All measurements were performed on solvent-cast films weighing 5.5 ± 0.5 mg. The temperature protocol employed in this study was adapted from established self-nucleation experiments described in the literature.[33,34] Initially, the samples were rapidly heated from 30 °C to 270 °C at a rate of 100 °C min$^{-1}$ and held at 270 °C for 3 minutes, as depicted in Fig. 1. Subsequently, the films were cooled to 30 °C at 10 °C min$^{-1}$, yielding different microstructures ranging from partially melted to isotropic melt states. The films were then subjected to various self-nucleation temperatures ($T_a$) ranging from 160 °C to 270 °C for 5 minutes to induce a diverse range of melt structures. The choice of $T_a$ exerted a significant influence on polymer crystallization, which was assessed by examining the crystallization peak temperatures ($T_c$) during the subsequent cooling process from $T_a$ to 30 °C, and melting temperatures ($T_m$) and melting enthalpies ($\Delta H_m$) during the subsequent heating process from 30 °C to 270 °C, both at a rate of 10 °C min$^{-1}$. The protocol was further modified to study the isothermal HC crystallization behavior under different $T_a$ and the state of SC-crystals, as shown in Fig. 1B. After cooling from $T_a$, the films were held at selected temperatures (140–160 °C) for 30 minutes. Each experiment was performed in duplicate, and it should be noted that the $T_c$ values demonstrated minimal deviation,[34] typically within the range of 1–2 °C.

## Results and discussion

Fig. 2A illustrates the heating curve of SCPLA after removing the thermal history through annealing at 270 °C for 3 minutes. The curve reflects the characteristic thermal behavior of high-molecular-weight SCPLA, displaying a pronounced melting
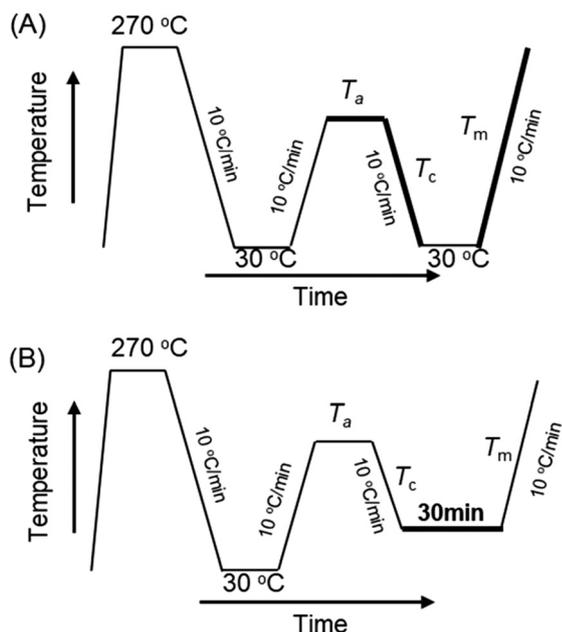
**Fig. 1** DSC temperature protocols for (A) nonisothermal and (B) isothermal crystallization after annealing at $T_a$.

peak c. 175 °C attributed to HC crystals and a less prominent melting peak associated with SC crystals, c. 220 °C.[4] The marked yellow area (186–242 °C) represents the annealing temperature range ($T_a$) investigated in this study. Fig. 2B shows the typical melting peak of HC-crystals and the crystallization peak temperature ($T_c$) obtained during homochiral PLA (HCPLA) cooling from various $T_a$ values. The self-nucleation behavior of semicrystalline homopolymers, including HCPLA, has been extensively studied.[34,35] Specifically, in this study, constant $T_c$ values are observed for $T_a > 180$ °C. Since $T_c$ is proportional to the nucleation density of crystallization, the constant $T_c$ values at $T_a > 180$ °C imply a constant concentration of nuclei, characterizing a heterogeneous nucleated crystalliza-

tion in an isotropic melt.[34] In this state, HC-crystals were fully melted without any residual melt memory, incurring self-nucleation effects, which otherwise would have promoted subsequent crystallization as evidenced by higher $T_c$ values observed at $T_a = 180$ °C. Consequently, the present study investigates the dependence of subsequent HC crystallization in SCPLA solely on the remaining SC-crystals at different states.

Fig. 3A presents the DSC cooling curves of SCPLA after annealing at different $T_a$ values, where the corresponding $T_a$ values were marked next to the respective curves. When $T_a < 220$ °C, only one exothermic peak was detected. At these lower temperatures, the SC-crystals undergo annealing and crystal perfection; thereby, the subsequent crystallization of SC during the cooling process might occur too rapidly to be detected by the instrument, as evidenced by the hardly visible exothermic peak at $T_a = 220$ °C. Since SC crystallization was too quick to be detected, the detected exothermic peak between 100 °C and 150 °C should be attributed to HC crystallization. At higher temperatures (226 °C $\leq T_a \leq$ 240 °C), SC-crystals are partially molten, resulting in the detection of two exothermal peaks during the cooling scans. As SC crystallization precedes HC crystallization, the peaks at higher and lower temperatures should be ascribed to SC and HC crystallization, respectively.[32,36] At higher $T_a$ ($\geq$246 °C, only 270 °C is shown for brevity), only one weak exothermic peak was observed and remained constant at around 101 °C. This temperature corresponds to the HC crystallization peak obtained by annealing HCPLA at $T_a \geq 190$ °C (Fig. 2B). Previous work using WAXS has also confirmed that only HC-crystals form during the nonisothermal crystallization of SCPLA from the isotropic melt at a cooling rate of 10 °C min$^{-1}$.[9] Therefore, the $T_c$ obtained for SCPLA annealed at high $T_a$ should be attributed to HC crystallization. Fig. 3B summarizes the relationship between the HC crystallization peak ($T_{c,HC}$) and the SC crystallization peak ($T_{c,SC}$) obtained at different $T_a$ values. As the HC-crystals have completely melted at these $T_a$ values, the variations in $T_{c,HC}$ indicate changes in the nucleation efficiency (NE) of pre-existing SC-crystals in influencing subsequent HC crystallization.
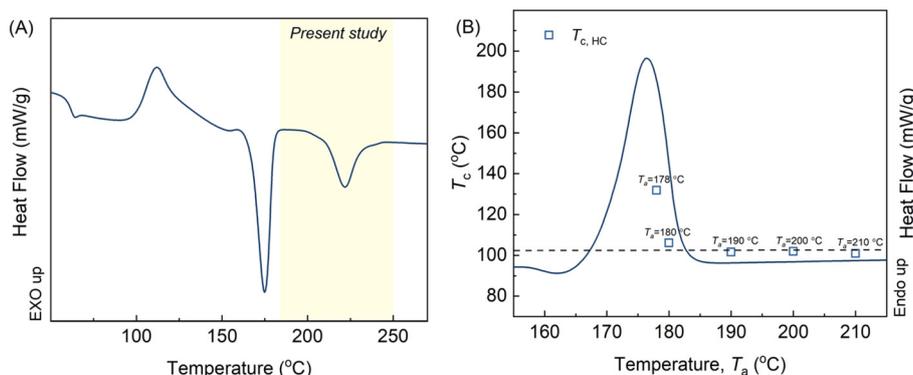


**Fig. 2** (A) DSC heating curve of SCPLA after cooling from 270 °C at 10 °C min$^{-1}$. The thermal history of the samples was first removed at 270 °C for 3 min. (B) Endothermic peak of HC-crystal melting for HCPLA and the crystallization peak temperatures ($T_{c,HC}$) during HCPLA cooling from different $T_a$ (as $x$-axis).
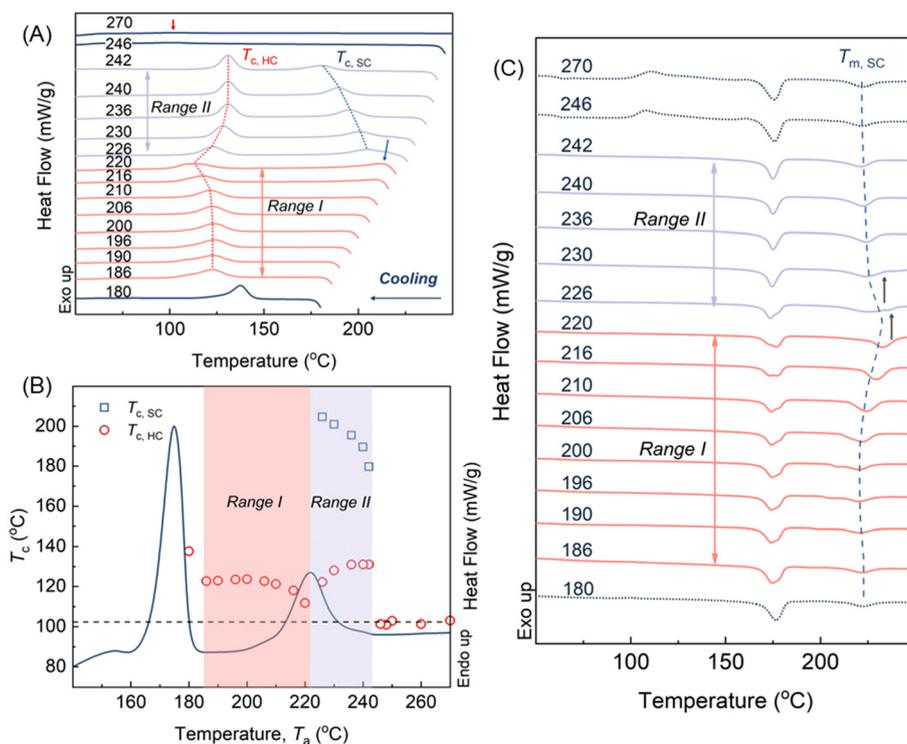
**Fig. 3** (A) DSC curves of SCPLA during cooling from different $T_a$ to 30 °C at 10 °C min$^{-1}$. (B) Corresponding $T_{c,HC}$ and $T_{c,SC}$ obtained from the DSC cooling curves. (C) Corresponding DSC heating curves from 30 °C to 270 °C at 10 °C min$^{-1}$ after the cooling from different $T_a$.

As proposed by Fillon *et al.*,[33] NE can be represented by eqn (1), where NE is proportional to $T_c$.

$$\text{NE} = \frac{T_c - T_c^{\min}}{T_c^{\max} - T_c^{\min}} \quad (1)$$

In the present study, $T_c^{\min}$ (101 °C) and $T_c^{\max}$ (132 °C) were obtained from Fig. 3B, representing the crystallization temperatures of the isotropic PLLA melt and the highest crystallization temperature of the self-nucleated PLLA melt, respectively. Consequently, NE of the SC-crystal on subsequent HC crystallization varied from 100% to nearly 0%, depending on the state of pre-existing SC-crystal at different $T_a$ values. Examining the state of pre-existing SC-crystal is crucial to gaining a deeper understanding of this phenomenon. Fig. 3C illustrates the DSC heating curves of SCPLA following subsequent crystallization cooling from different $T_a$ values, as denoted next to the respective curves. At higher $T_a$ values ($\geq$246 °C), both the constant $T_{c,HC}$ values (Fig. 3B) and the melting peak of the SC-crystal ($T_{m,SC}$) (Fig. 3C) demonstrate the typical crystallization behavior of high-molecular-weight SCPLA. Under these $T_a$ conditions, the SCPLA was in an isotropic melt state, and pre-existing crystals were completely melted without any melt memory. Consequently, predominantly HC-crystals were formed during subsequent crystallization, as observed in Fig. 3C. Conversely, at the lower $T_a$ value of 180 °C, the temperature was too low to melt the HC-crystal fully, and the subsequent crystallization behavior was influenced by both the remaining HC-crystal and

the SC-crystal. This resulted in the highest NE ($T_{c,HC}$) among the studied $T_a$ temperatures. As mentioned above, the present study solely focuses on the dependence of subsequent HC crystallization in SCPLA on the remaining SC-crystals at different states; therefore, the following discussion is confined between 180 °C < $T_a$ < 246 °C. For the sake of conciseness, the temperature ranges are further divided into two categories: range I and II. This division is solely for simplification and should not be mistaken for self-nucleation domains.[34]

In the range I, the $T_{c,HC}$ (Fig. 3B) firstly remains constant. Fig. 3C also demonstrates that the $T_{m,SC}$ remain unchanged. This suggests that, although SC crystallization occurs during annealing, pre-existing SC-crystals do not undergo further thickening, as confirmed by the consistent SAXS pattern and intensified SC diffraction pattern collected *in situ* during heating of solvent-cast SCPLA (Fig. S1A and S1B available in the SI). Besides, two melting peaks were observed for HC-crystal melting around 175 °C in Fig. 3C, which may have originated from incomplete HC crystallization during cooling from $T_a$ and the crystallization during DSC scanning. Such phenomenon diminished at high $T_a$ > 220 °C (range II), indicating a temperature effect on the HC crystallization that is further elaborated in the following section. Further increasing annealing temperature in range II, the $T_{c,HC}$ decreases and reaches its lowest value at $T_a$ = 220 °C, corresponding to the constraint in NE. Fig. 3C shows an increase in $T_{m,SC}$ with the increasing $T_a$ values, indicating the thickening of pre-existing SC-crystals during annealing, as also evidenced by the shift of the SAXS

peak to lower $q$ during *in situ* measurements (Fig. S1C and S1D available in the SI). The SC crystallinity reached a maximum after annealing at 220 °C. This phenomenon may indicate the correlation between $T_{c,HC}$, and SC crystallinity, as discussed in the following section. Increasing the annealing temperature into the range II leads to the development of $T_{c,SC}$ (Fig. 3B), indicating the occurrence of SC crystallization during cooling from the associated $T_a$ due to the considerable melting of SC-crystals. However, the SC-crystals may partially melt, and the remaining crystal or crystal fragments can serve as nuclei or seeds for subsequent crystallization.[34] The concentration of remaining SC-crystal or crystal fragments that act as nucleators for subsequent SC crystallization decreases with increasing $T_a$, reducing the $T_{c,SC}$.[35] However, such variation in the concentration of SC-crystal or its fragments does not influence the subsequent $T_{c,HC}$, which seems to contradict the above-mentioned possible correlation between SC crystallinity and $T_{c,HC}$.

To understand the effect of concentration of SC-crystal or crystal fragments on the $T_{c,HC}$, SCPLA annealed at different $T_a$ for 30 minutes is compared with annealing for 5 minutes. Fig. 4A illustrates the melting enthalpy of HC and SC-crystals ($\Delta H_{m,HC}$ and $\Delta H_{m,SC}$) obtained after subsequent crystallization. Due to the increased degree of crystallization with prolonged annealing time to 30 min, the $\Delta H_{m,SC}$ values were increased between 180 and 220 °C compared to that from 5 min. This effect is particularly prominent at $T_a$ = 220 °C, where the highest crystallization is located. At $T_a$ values above 220 °C, the similarity between $\Delta H_{m,SC}$ obtained from 5 min and 30 min of annealing indicates that most of the crystals have melted, with only a few thickened SC-crystals may survive, resulting in limited changes in $\Delta H_{m,SC}$ at the two different annealing times. For both 5 min and 30 min annealing times, across the entire range of $T_a$ values, a higher $\Delta H_{m,SC}$ is associated with a lower $\Delta H_{m,HC}$, and *vice versa*. This indicates that the concentration of pre-existing SC crystals (crystallinity) significantly influences subsequent HC crystallization. To further support this, FTIR imaging was used to provide complementary chemical and morphological information to the DSC data, thereby supporting the observed inverse relationship between

SC and HC crystallisation at $T_a$ values of 190 °C and 220 °C (Fig. S2; Table SI). Interestingly, Fig. 4B shows that although $T_{c,HC}$ varies with $T_a$, the magnitude of this variation is relatively small when compared to the substantial changes in SC-crystal concentration observed in Fig. 4A for 180 °C < $T_a$ < 210 °C and 230 °C < $T_a$ < 250 °C. This suggests that while the SC-crystal state and its nucleation effectiveness are indeed temperature-dependent, the concentration of pre-existing SC crystals and fragments predominantly influences the crystal-growth process ($\Delta H_{m,HC}$), whereas its impact on the nucleation density reflected by $T_{c,HC}$ is comparatively slight.

As pre-existing SC-crystal demonstrated a different influence in subsequent nonisothermal HC crystal growth and nucleation, the isothermal HC crystallization under different $T_a$ was also investigated to add to the understanding of the root cause. Fig. 5A and B selectively display the DSC traces during isothermal crystallization at various temperatures and the subsequent heating after cooling from $T_a$ = 220 °C. No obvious exothermic peaks were observed during the isothermal treatment at 160 °C (Fig. 5A). Moreover, a pronounced HC-crystal melting peak was absent in the heating curves (Fig. 5B). These observations imply a minimal extent of HC or SC crystallization that occurred during the isothermal process at 160 °C. Therefore, the melting enthalpy of the SC-crystal obtained during isothermal at 160 °C equals the amount of SC-crystal formed at that $T_a$. Fig. 5B also demonstrates that the melting enthalpy of the SC-crystal remains independent of the isothermal crystallization temperatures. This indicates that the observed exothermal peaks (Fig. 5A) during isothermal treatment should be attributed solely to HC crystallization. Fig. 5C and D present the crystallization half-time and Avrami exponent $n$ obtained from Avrami analysis on the HC-crystallization exothermal peak.[37,38] The crystallization half-time serves as an indication of the overall crystallization rate. Hence, the degree of supercooling ($T_{m,0}-T_c$) required to achieve a similar crystallization rate varies with different $T_a$ values. Specifically, samples annealed at $T_a$ = 220 °C require a higher degree of supercooling. By extrapolating the curves to the same temperature, one can evaluate the crystallization rate of the systems after anneal-
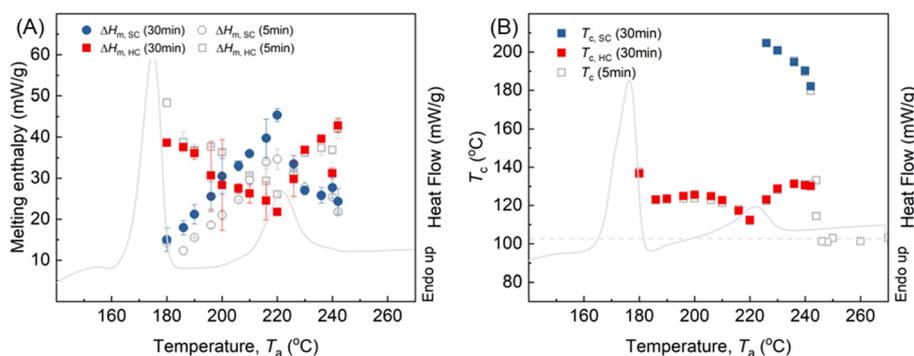


**Fig. 4** (A) Melting enthalpies of HC ($\Delta H_{m,HC}$) and SC-crystals ($\Delta H_{m,SC}$) of SCPLA obtained upon cooling from different $T_a$ for 5 min (empty symbols) or 30 min (solid symbols). (B) The corresponding $T_c$ values of HC and SC-crystallization of SCPLA during cooling from different $T_a$ for 5 min (empty symbols) or 30 min (solid symbols).
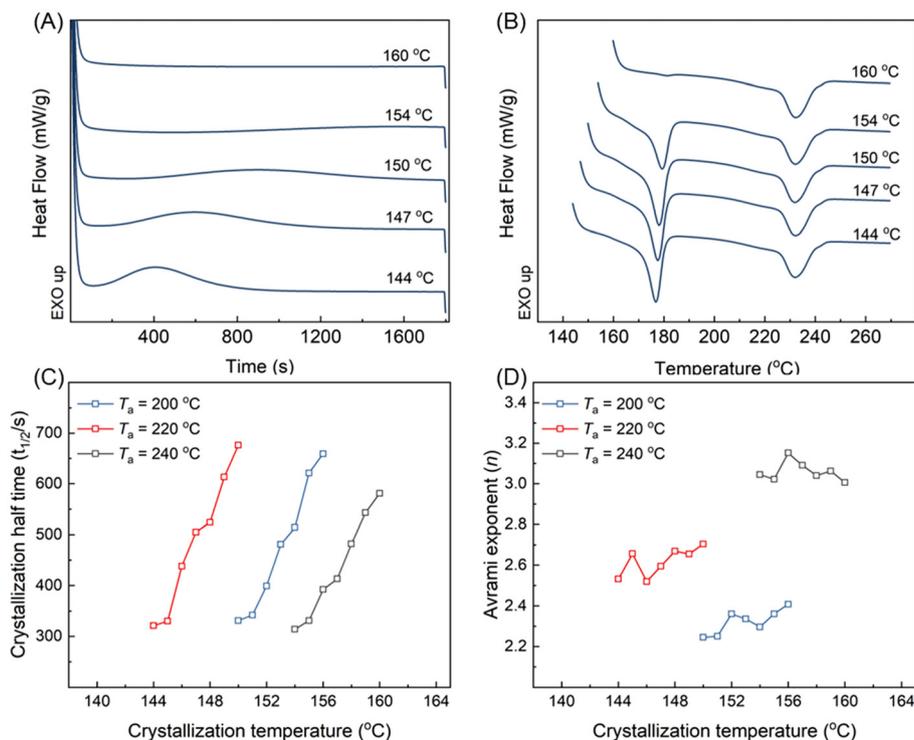
**Fig. 5** DSC curves of SCPLA (A) during isothermal crystallization at different temperatures after annealing at $T_a$ = 220 °C and (B) subsequent heating curves. (C) Crystallization half-time and (D) Avrami exponent of SCPLA isothermal crystallization at different temperatures after annealing at different $T_a$ as denoted.

ing at the three different $T_a$ values.[39] Compared to $T_a$ = 240 °C, the overall crystallization rate of HC crystallization is suppressed after annealing at $T_a$ = 200 and 220 °C.

The Avrami exponent $n$ is often used to indicate the nucleation mechanism and crystal growth dimension.[40] Depending on the growth dimension from 1D to 3D, the crystal growth dimension contributes a value of 1 to 3 to the exponent. The nucleation mode contributes a value of 0 and 1 to the exponent for heterogeneous and homogeneous nucleation, respectively. However, homogenous nucleation may not be applied in the present study as it requires conditions such as high supercooling or the presence of microdomains within small droplets.[30] As shown in Fig. 5D, annealing at $T_a$ = 240 °C resulted in Avrami exponents ranging from 3.0 to 3.2, indicating simultaneous nucleation and 3D spherulitic crystal growth, commonly observed in heterogeneously nucleated polymer crystallization without confinement. Interestingly, at $T_a$ = 220 and 200 °C, the Avrami exponent decreased to the range of 2.4–2.8 and 2.2–2.4, respectively, indicating confinement effects on HC crystallization. Similar observations have been reported in the systems with geometrical constraints[41,42] or restricted diffusion.[43,44] As discussed earlier, the concentration of SC-crystals does not affect the nucleation density of HC crystallization, ruling out geometrical constraints imposed by pre-existing SC-crystals as the cause for the reduction in Avrami exponent. Although a higher concentration of SC-crystals can suppress crystal growth (Fig. 4), the crystal growth dimension

should remain unaltered, as evidenced by $T_a$ = 220 °C having higher Avrami exponents than $T_a$ = 200 °C, despite the higher concentration of pre-existing SC-crystals. Another possibility is that the diffusion of homopolymer chains for HC crystallization is restricted[44] after annealing at temperatures below 220 °C in the studied temperature range. The underlying mechanism is further discussed in the subsequent section.

To investigate the potential contribution of diffusion effects to HC crystallization, self-nucleation experiments were performed using plasticized SCPLA with 2 wt% PEG (PEG2) following the same protocol. Fig. 6 illustrates the $T_c$ and the melting enthalpies of SC and HC crystals under different $T_a$ for PEG2, compared to SCPLA. A selective reduction in $T_{c,HC}$ was observed at range I ($T_a \leq 220$ °C) in Fig. 6A, suggesting that a diffusion barrier may be present at those temperatures. In SC-nucleated HC crystallization, favorable interactions between SC-crystals and amorphous PLA chains are believed to play a crucial role.[15] Within the SCPLA melt, the self-concentration of same-chiral segments and the mixing of racemate segments occur spontaneously due to thermal fluctuations.[7,9] This local competition may dictate the HC and SC crystallization competition.

On the other hand, driven by the selection progress of SC crystallization, racemate pairing flourishes near the growth front of nuclei, forming SC helices or precursors.[9,28,31] Closer look at the chain conformation by flash-DSC and micro-FTIR methodologies by Zhang *et al.*[31] suggested the coexistence of

**656** | *RSC Appl. Polym.*, 2026, **4**, 651–661

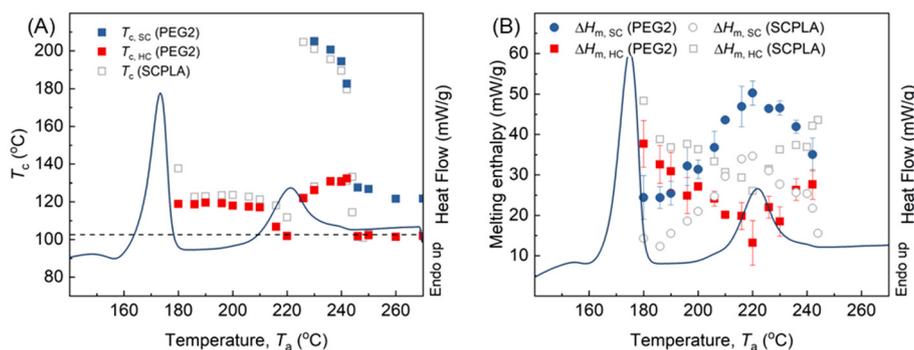© 2026 The Author(s). Published by the Royal Society of Chemistry

**Fig. 6** The $T_a$ correspondence of (A) $T_c$ and (B) melting enthalpies for plasticized SCPLA blend with 2 wt% PEG (labelled PEG2) as compared to neat SCPLA (labelled SCPLA). The error bars are not presented because of low measurement deviation.

$10_3$ helices and $3_1$ helices in the melt before crystallization. Moreover, the $10_3$ helix should emerge first and gradually transform to the $3_1$ SC helix driven by hydrogen bonding.[31] The source of $10_3$ helix may originate from multiple events, such as the uncrystallized segments of intermolecular nucleation and the rejection of the selection process.[32] As a result, the probability of interaction between neighboring $10_3$ helices increases, promoting the HC nucleation. Since the matrix comprises equivalent random PLLA and PDLA coils, the enriched $10_3$ (either in PLLA or PDLA) may tend to homogenize into the matrix conformation driven by thermal fluctuation and concentration gradient. This homogenization process may be in a dynamic equilibrium with the aggregation process of $10_3$ and $3_1$ helices driven by crystallization. Chain diffusion may control the homogenization progress; hence, high chain mobility may intensify the homogenization, resulting in fewer $10_3$ helices and thereby lower $T_{c,HC}$, as evidenced by the lower $T_{c,HC}$ at higher $T_a$. In the case of the PEG-plasticized system,[45] the plasticization effect can also facilitate homogenization, causing lower $T_{c,HC}$ than unplasticized SCPLA. Additionally, since the selection process of SC crystallization, PEG may be rejected from the local region near the growth front, and a composition gradient may exist to further drive the homogenization from local region composition to matrix composition.

At range II, $T_a$ between 220–242 °C, compared to SCPLA, PEG addition does not affect the HC nucleation but promotes SC nucleation, as evidenced by the increase in $T_{c,SC}$ (Fig. 6A). The unchanged $T_{c,HC}$ after PEG addition indicates the disappearance of the diffusion control to homogenization, and the nucleation behavior is governed by the survived SC-crystals or fragments at different $T_a$. SC-crystals or fragments can serve as seeds for subsequent crystallization, leading to increased $T_{c,SC}$ with the concentration of survived SC-crystal or fragments. Fig. 6B also shows a significant improvement in $\Delta H_{m,SC}$ by PEG addition, which can be attributed to faster crystal growth in the presence of a plasticizer.[8] The higher SC-crystallinity in PEG2 can thus lead to higher concentrations of survived SC-crystal and fragments, demonstrating the elevated $T_{c,SC}$ in PEG2. Moreover, as the pre-existing SC-crystals melt and recrystallize at those high $T_a$,[46] homogenization is mainly

driven by temperature and is more complete. In this context, extra plasticization from PEG may not further contribute to the saturated homogenization, resulting in similar $T_{c,HC}$ in PEG2 with unplasticized SCPLA. On the other hand, the general increase in $T_{c,HC}$ with $T_a$ can be attributed to the enriched $10_3$ helix formed during SC crystallization at lower $T_{c,SC}$. Additionally, at $T_a > 242$ °C corresponding to isotropic melt, as discussed before, the $T_{c,HC}$ remains the same as neat SCPLA, whereas the $T_{c,SC}$ appears around 120 °C, which is simply because of the well-known PEG promotion effect on SC-crystallization.[8]

To further investigate the homogenization process during SC-nucleated HC crystallization, asymmetric blends with a PLLA : PDLA ratio of 90 : 10 (L90) were employed using the same self-nucleation procedure. Fig. 7A illustrates the correlation between $T_c$ and $T_a$, while Fig. 7B shows the corresponding melting enthalpies of SC and HC crystals after the crystallization during cooling. Despite a lower concentration of pre-existing SC-crystals in L90 (Fig. 7B), HC nucleation was still promoted, with $T_{c,HC}$ falling within a similar range as that of symmetric SCPLA in Fig. 7A. This observation can be attributed to the saturation of the "nucleating agent" concentration, as previously observed in asymmetric SCPLA.[19] Interestingly, in contrast to PEG2, the variations in $T_{c,HC}$ for L90 samples were primarily altered at $T_a > 220$ °C, while the $T_{c,HC}$ in the diffusion-controlled region ($T_a \leq 220$ °C) showed less influence from the asymmetric composition. As discussed earlier, the $10_3$ helices can enrich near the growth front and act as nuclei for HC crystallization, and the dynamic balance between homogenization and crystallization-driven aggregation determines the concentration. At $T_a \leq 220$ °C, the homogenization is suppressed; the local region of L90 may be close to a symmetric 1 : 1 composition due to the helix selection of SC crystallization to the paired racemic PLLA/PDLA.[30,47–49] Therefore, the asymmetric composition of L90 incurred a slight increase on $T_{c,HC}$. This slight increase can be linked to the composition gradient in L90 compared to symmetric SCPLA, where L90 has a local region composition closer to symmetry and a matrix region enriched with PLLA. The higher composition gradient selectively drives more homopolymer PLLA to diffuse towards the
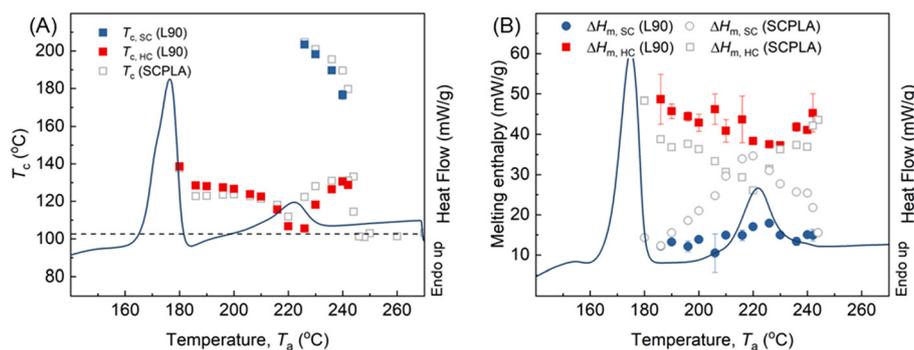
© 2026 The Author(s). Published by the Royal Society of Chemistry

*RSC Appl. Polym.*, 2026, **4**, 651–661 | **657**

**Fig. 7** The $T_a$ correspondence of (A) $T_c$ and (B) melting enthalpies for the asymmetric SCPLA blend (PLLA : PDLA = 90 : 10 wt%) as compared to the symmetric SCPLA.

local regions, resulting in a slightly higher $T_{c,HC}$. At higher $T_a$ approaching 220 °C, the great extent of conformation homogenization reduced the overall concentration of $10_3$ helices; therefore, the impact of composition difference decreased. Increasing $T_a$ to >220 °C, the lower $T_{c,HC}$ in L90 than symmetric SCPLA indicates fewer $10_3$ helices formed during subsequent SC-crystallization in L90. As the diffusion barrier for homogenization disappeared at those high $T_a$, the local regions in L90 adapted the matrix composition in PLLA : PDLA 9 : 1. This might have resulted in a lower concentration of $3_1$ helices and, consequently, attracted fewer $10_3$ helices by hydrogen bonding[31] during homogenization progress in the subsequent SC crystallization. However, this effect can be neglected when SC-crystallization occurs at lower temperatures ($T_{c,SC}$) where enough $10_3$ helices are aggregated due to suppressed homogenization, as evidenced by less $T_{c,HC}$ changes in L90 at higher $T_a$ around 236 to 242 °C.

The proposed mechanisms of SC-nucleated HC crystallization and their influence on the phenomena observed in this study are summarized in Fig. 8. During the early stages of crystallization, before PLA segments attach to the nuclei (SC crystals), two chain conformations ($10_3$ and $3_1$ helices) may coexist

and become enriched in local regions surrounding the nuclei.[31] This early aggregation is driven by nucleation-selection processes (acceptance or rejection of chains) and by hydrogen-bonding interactions. While SC crystallization consumes a fraction of the $3_1$ helices, the remaining $10_3$ helices serve as effective seeds for subsequent HC crystallization. Thermal fluctuations and composition gradients simultaneously promote homogenization of the local environment, guiding it toward the overall matrix composition and chain conformation.

In our proposed mechanism, the accumulation of $10_3$ helices near the crystal growth front plays a decisive role in determining whether SC or HC crystals preferentially nucleate. The $10_3$ helix provides a local conformational environment that facilitates the alignment of enantiomeric PLLA and PDLA chains, thereby lowering the nucleation barrier for SC formation. When $10_3$ helices reach sufficiently high local density, they promote stable interchain packing and thus enhance SC nucleation efficiency. Conversely, when the density of $10_3$ helices is low or spatially heterogeneous, the cooperative pre-organization required for SC formation is weakened, making HC nucleation more favorable. Consequently, the balance between SC and HC crystallization is governed by the extent of $10_3$-helix enrichment at the growth front and its ability to prearrange chains for stereocomplexation.

The concentration of $10_3$ helices is set by a dynamic equilibrium between crystallization-driven aggregation and homogenization driven by thermal fluctuations and composition gradients. This equilibrium is diffusion-controlled. At low annealing temperatures ($T_a \leq 220$ °C), where SC crystallization dominates, homogenization is suppressed, leading to strong local aggregation of both $10_3$ and $3_1$ helices. Although some $3_1$ helices are consumed during SC formation, the remaining $10_3$ helices efficiently promote HC nucleation, resulting in a high $T_{c,HC}$. Increasing $T_a$ or adding plasticizer enhances chain mobility, strengthens homogenization, and consequently reduces $T_{c,HC}$. At higher $T_a$ (>220 °C), where SC crystals melt and homogenization prevails, the local composition becomes fully adapted to that of the matrix.
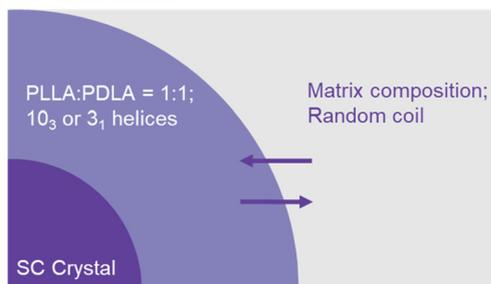


**Fig. 8** The schematic diagram of homogenization progress during SC-crystallization, where the $10_3$ or $3_1$ helices enriched near the growth front of SC-crystals tend to homogenize into the matrix in both its composition and conformation.

© 2026 The Author(s). Published by the Royal Society of Chemistry

In such scenarios, a high PLLA ratio in L90 demonstrated lower $T_{c,HC}$ than SCPLA with symmetric composition. This may be because the local PLLA : PDLA 9 : 1 composition hinders the formation of $3_1$ helices, resulting in fewer $10_3$ helices surviving with less hydrogen bonding. The aggregation of $10_3$ and $3_1$ helices, on the other hand, retards the diffusion of homopolymer from the matrix onto the growth front of HC-nuclei during isothermal crystallization, and consequently, showing reduced Avrami exponents and two HC-crystal melting peaks as shown in Fig. 3C due to the suppressed or incomplete HC-crystallization.

## Conclusion

This study reported the nonisothermal and isothermal stereo-complex (SC)-nucleated homochiral (HC) crystallization behavior by creating different states of pre-existing SC crystals at various annealing temperatures ($T_a$), adapting the classic self-nucleation experiments. The HC crystallization temperatures during nonisothermal crystallization were found to be temperature-dependent rather than dependent on pre-existing SC crystallinity. Specifically, NE decreased with $T_a$ at lower temperatures ($T_a \leq 220$ °C), while it increased with $T_a$ at higher temperatures ($T_a > 220$ °C). The minimum of NE was found at $T_a = 220$ °C, where the SC crystallization proceeds at the highest rate. The application of Avrami analysis for isothermal crystallization revealed variations in crystallization half-time and Avrami exponents with $T_a$. Notably, the slowest overall HC crystallization rate was observed after annealing at $T_a = 220$ °C, which could be attributed to the suppression of crystal growth by the highest pre-existing SC crystallinity. Additionally, a decrease in Avrami exponents was observed for samples annealed at $T_a = 200$ and 220 °C compared to $T_a = 240$ °C, indicating diffusion-controlled crystallization. Furthermore, the addition of PEG as a plasticizer altered the NE. At $T_a \leq 220$ °C, NE decreased compared to unplasticized SCPLA, further indicating diffusion-controlled progress. Conversely, L90 with asymmetric composition displayed lower NE than symmetric SCPLA, mainly at $T_a > 220$ °C, suggesting that equilibrium of the diffusion can be achieved at higher temperatures. To understand the intricate behaviors, this study proposed that the nucleation of HC crystallization is linked to the concentration of $10_3$ helices remaining after the prior SC-crystallization. This concentration may be governed by a dynamic equilibrium between homogenization and aggregation, with the homogenization being a diffusion-controlled, thermal fluctuation and composition gradient-driven process, and the aggregation being a crystallization-driven process. These findings provide new insights into the complex interplay between SC and HC crystallization and an approach to designing polymorphic polymer materials.

## Conflicts of interest

The authors do not have any conflicts of interest to declare.

## Data availability

The data supporting this article have been included as part of the supplementary information (SI). Supplementary information is available. See DOI: https://doi.org/10.1039/d4lp00319e.

## Acknowledgements

## References

1 H. Tsuji, Poly(lactic acid) stereocomplexes: A decade of progress, *Adv. Drug Delivery Rev.*, 2016, **107**, 97–135.

2 Q. Chen, R. Auras, J. J. K. Kirkensgaard and I. Uysal-Unalan, Modulating Barrier Properties of Stereocomplex Polylactide: The Polymorphism Mechanism and Its Relationship with Rigid Amorphous Fraction, *ACS Appl. Mater. Interfaces*, 2023, **15**(42), 49678–49688.

3 Q. Chen, R. Auras and I. Uysal-Unalan, Role of stereocomplex in advancing mass transport and thermomechanical properties of polylactide, *Green Chem.*, 2022, **24**(9), 3416–3432.

4 Y. Ikada, K. Jamshidi, H. Tsuji and S. H. Hyon, Stereocomplex formation between enantiomeric poly(lactides), *Macromolecules*, 1987, **20**(4), 904–906.

5 J. Liu, X. Qi, Q. Feng and Q. Lan, Suppression of phase separation for exclusive stereocomplex crystallization of a high-molecular-weight racemic poly (L-lactide)/poly (D-lactide) blend from the glassy state, *Macromolecules*, 2020, **53**(9), 3493–3503.

6 H. Tsuji, S. H. Hyon and Y. Ikada, Stereocomplex formation between enantiomeric poly(lactic acid)s. 3. Calorimetric studies on blend films cast from dilute solution, *Macromolecules*, 1991, **24**(20), 5651–5656.

7 Y. He, D. Liu, J. Wang, P. Pan and W. Hu, Tammann Analysis of the Molecular Weight Selection of Polymorphic Crystal Nucleation in Symmetric Racemic Poly(lactic acid) Blends, *Macromolecules*, 2022, **55**(9), 3661–3670.

8 R.-Y. Bao, W. Yang, X.-F. Wei, B.-H. Xie and M.-B. Yang, Enhanced Formation of Stereocomplex Crystallites of High Molecular Weight Poly(l-lactide)/Poly(d-lactide) Blends from Melt by Using Poly(ethylene glycol), *ACS Sustainable Chem. Eng.*, 2014, **2**(10), 2301–2309.

9 Q. Chen, R. Auras, M. Corredig, J. J. K. Kirkensgaard, A. Mamakhel and I. Uysal-Unalan, New opportunities for sustainable bioplastic development: Tailorable polymorphic and three-phase crystallization of stereocomplex polylactide by layered double hydroxide, *Int. J. Biol. Macromol.*, 2022, **222**, 1101–1109.

© 2026 The Author(s). Published by the Royal Society of Chemistry

*RSC Appl. Polym.*, 2026, **4**, 651–661 | **659**

10  L. Han, P. Pan, G. Shan and Y. Bao, Stereocomplex crystallization of high-molecular-weight poly(l-lactic acid)/poly(d-lactic acid) racemic blends promoted by a selective nucleator, *Polymer*, 2015, **63**, 144–153.

11  H. Urayama, T. Kanamori, K. Fukushima and Y. Kimura, Controlled crystal nucleation in the melt-crystallization of poly(l-lactide) and poly(l-lactide)/poly(d-lactide) stereocomplex, *Polymer*, 2003, **44**(19), 5635–5641.

12  Y. Song, X. Zhang, Y. Yin, S. de Vos, R. Wang, C. A. P. Joziasse, G. Liu and D. Wang, Enhancement of stereocomplex formation in poly(l-lactide)/poly(d-lactide) mixture by shear, *Polymer*, 2015, **72**, 185–192.

13  H. Tsuji, H. Takai and S. K. Saha, Isothermal and non-isothermal crystallization behavior of poly(l-lactic acid): Effects of stereocomplex as nucleating agent, *Polymer*, 2006, **47**(11), 3826–3837.

14  S. Saeidlou, M. A. Huneault, H. Li and C. B. Park, Effect of nucleation and plasticization on the stereocomplex formation between enantiomeric poly(lactic acid)s, *Polymer*, 2013, **54**(21), 5762–5770.

15  S. C. Schmidt and M. A. Hillmyer, Polylactide stereocomplex crystallites as nucleating agents for isotactic polylactide, *J. Polym. Sci., Part B: Polym. Phys.*, 2001, **39**(3), 300–313.

16  K. S. Anderson and M. A. Hillmyer, Melt preparation and nucleation efficiency of polylactide stereocomplex crystallites, *Polymer*, 2006, **47**(6), 2030–2035.

17  N. Ji, G. Hu, J. B. Li and J. Ren, Influence of poly(lactide) stereocomplexes as nucleating agents on the crystallization behavior of poly(lactide)s, *RSC Adv.*, 2019, **9**(11), 6221–6227.

18  J. Narita, M. Katagiri and H. Tsuji, Highly Enhanced Nucleating Effect of Melt-Recrystallized Stereocomplex Crystallites on Poly(L-lactic acid) Crystallization, *Macromol. Mater. Eng.*, 2011, **296**(10), 887–893.

19  X.-F. Wei, R.-Y. Bao, Z.-Q. Cao, W. Yang, B.-H. Xie and M.-B. Yang, Stereocomplex Crystallite Network in Asymmetric PLLA/PDLA Blends: Formation, Structure, and Confining Effect on the Crystallization Rate of Homocrystallites, *Macromolecules*, 2014, **47**(4), 1439–1448.

20  J. Narita, M. Katagiri and H. Tsuji, Highly Enhanced Accelerating Effect of Melt-Recrystallized Stereocomplex Crystallites on Poly(L-lactic acid) Crystallization, 2–Effects of Poly(D-lactic acid) Concentration, *Macromol. Mater. Eng.*, 2013, **298**(3), 270–282.

21  J. Narita, M. Katagiri and H. Tsuji, Highly enhanced accelerating effect of melt-recrystallized stereocomplex crystallites on poly(L-lactic acid) crystallization: effects of molecular weight of poly(D-lactic acid), *Polym. Int.*, 2013, **62**(6), 936–948.

22  Z.-C. Zhang, X.-R. Gao, Z.-J. Hu, Z. Yan, J.-Z. Xu, L. Xu, G.-J. Zhong and Z.-M. Li, Inducing Stereocomplex Crystals by Template Effect of Residual Stereocomplex Crystals during Thermal Annealing of Injection-Molded Polylactide, *Ind. Eng. Chem. Res.*, 2016, **55**(41), 10896–10905.

23  Y.-F. Huang, Z.-C. Zhang, Y. Li, J.-Z. Xu, L. Xu, Z. Yan, G.-J. Zhong and Z.-M. Li, The Role of Melt Memory and Template Effect in Complete Stereocomplex Crystallization and Phase Morphology of Polylactides, *Cryst. Growth Des.*, 2018, **18**(3), 1613–1621.

24  N. Rahman, T. Kawai, G. Matsuba, K. Nishida, T. Kanaya, H. Watanabe, H. Okamoto, M. Kato, A. Usuki, M. Matsuda, K. Nakajima and N. Honma, Effect of Polylactide Stereocomplex on the Crystallization Behavior of Poly(l-lactic acid), *Macromolecules*, 2009, **42**(13), 4739–4745.

25  T. Lv, J. Li, S. Huang, H. Wen, H. Li, J. Chen and S. Jiang, Synergistic effects of chain dynamics and enantiomeric interaction on the crystallization in PDLA/PLLA mixtures, *Polymer*, 2021, **222**, 123648.

26  T. Wen, Z. Xiong, G. Liu, X. Zhang, S. de Vos, R. Wang, C. A. P. Joziasse, F. Wang and D. Wang, The inexistence of epitaxial relationship between stereocomplex and α crystal of poly(lactic acid): Direct experimental evidence, *Polymer*, 2013, **54**(7), 1923–1929.

27  B. Wang, T. Wen, X. Zhang, A. Tercjak, X. Dong, A. J. Müller, D. Wang and D. Cavallo, Nucleation of Poly(lactide) on the Surface of Different Fibers, *Macromolecules*, 2019, **52**(16), 6274–6284.

28  C.-F. Yang, Y.-F. Huang, J. Ruan and A.-C. Su, Extensive Development of Precursory Helical Pairs Prior to Formation of Stereocomplex Crystals in Racemic Polylactide Melt Mixture, *Macromolecules*, 2012, **45**(2), 872–878.

29  Y. Lu, D. Lyu, X. Zhao and Y. Men, Influence of Molecular Weight on the Nucleation and Growth of Different Crystal Forms in Isotactic Polypropylene: In Situ Synchrotron Microfocus X-Ray Scattering Combined with Fast-Scanning Chip Calorimetry Investigations, *Macromolecules*, 2023, **56**(7), 2772–2780.

30  B. Lotz, T. Miyoshi and S. Z. D. Cheng, 50th Anniversary Perspective: Polymer Crystals and Crystallization: Personal Journeys in a Challenging Research Field, *Macromolecules*, 2017, **50**(16), 5995–6025.

31  M. Zhang, X. Fan, W. Guo, H. Zhou, Z. Li, Y. Ma, C. Yan and A. Dufresne, Insights into Stereocomplexation of Poly(lactic acid) Materials: Evolution of Interaction between Enantiomeric Chains and Its Role in Conformational Transformation in Racemic Blends, *ACS Appl. Polym. Mater.*, 2022, **4**(8), 5891–5900.

32  J. Cui, S.-G. Yang, Q. Zhang, F. Liu and G. Ungar, Poisoning by Purity: What Stops Stereocomplex Crystallization in Polylactide Racemate?, *Macromolecules*, 2023, **56**(3), 989–998.

33  B. Fillon, J. C. Wittmann, B. Lotz and A. Thierry, Self-nucleation and recrystallization of isotactic polypropylene (α phase) investigated by differential scanning calorimetry, *J. Polym. Sci., Part B: Polym. Phys.*, 1993, **31**(10), 1383–1393.

34  L. Sangroniz, D. Cavallo and A. J. Müller, Self-Nucleation Effects on Polymer Crystallization, *Macromolecules*, 2020, **53**(12), 4581–4604.

35  A. Jalali, M. A. Huneault and S. Elkoun, Effect of thermal history on nucleation and crystallization of poly(lactic acid), *J. Mater. Sci.*, 2016, **51**(16), 7768–7779.

36 P. Pan, L. Han, J. Bao, Q. Xie, G. Shan and Y. Bao, Competitive Stereocomplexation, Homocrystallization, and Polymorphic Crystalline Transition in Poly(l-lactic acid)/Poly(d-lactic acid) Racemic Blends: Molecular Weight Effects, *J. Phys. Chem. B*, 2015, **119**(21), 6462–6470.

37 A. T. Lorenzo, M. L. Arnal, J. Albuerne and A. J. Müller, DSC isothermal polymer crystallization kinetics measurements and the use of the Avrami equation to fit the data: Guidelines to avoid common problems, *Polym. Test.*, 2007, **26**(2), 222–231.

38 M. Avrami, Granulation, Phase Change, and Microstructure Kinetics of Phase Change. III, *J. Chem. Phys.*, 2004, **9**(2), 177–184.

39 X. Wen, Y. Su, Y. Shui, W. Zhao, A. J. Müller and D. Wang, Correlation between Grafting Density and Confined Crystallization Behavior of Poly(ethylene glycol) Grafted to Silica, *Macromolecules*, 2019, **52**(4), 1505–1516.

40 M. E. Taverna, A. S. Altorbaq, S. K. Kumar, J. L. Olmedo-Martínez, C. A. Busatto, M. Zubitur, A. Mugica, V. V. Nicolau, D. A. Estenoz and A. J. Müller, Supernucleation Dominates Lignin/Poly(ethylene oxide) Crystallization Kinetics, *Macromolecules*, 2022, **55**(17), 7663–7673.

41 M. Trujillo, M. L. Arnal, A. J. Müller, S. Bredeau, D. Bonduel, P. Dubois, I. W. Hamley and V. Castelletto, Thermal Fractionation and Isothermal Crystallization of Polyethylene Nanocomposites Prepared by in Situ Polymerization, *Macromolecules*, 2008, **41**(6), 2087–2095.

42 R. M. Michell and A. J. Müller, Confined crystallization of polymeric materials, *Prog. Polym. Sci.*, 2016, **54–55**, 183–213.

43 B. S. Hsiao, I. Y. Chang and B. B. Sauer, Isothermal crystallization kinetics of poly(ether ketone ketone) and its carbon-fibre-reinforced composites, *Polymer*, 1991, **32**(15), 2799–2805.

44 B. Wunderlich, *Macromolecular physics V2*, Elsevier, 2012.

45 F. Hassouna, J.-M. Raquez, F. Addiego, P. Dubois, V. Toniazzo and D. Ruch, New approach on the development of plasticized polylactide (PLA): Grafting of poly(ethylene glycol) (PEG) via reactive extrusion, *Eur. Polym. J.*, 2011, **47**(11), 2134–2144.

46 T. Lv, C. Zhou, J. Li, S. Huang, H. Wen, Y. Meng and S. Jiang, New insight into the mechanism of enhanced crystallization of PLA in PLLA/PDLA mixture, *J. Appl. Polym. Sci.*, 2018, **135**(2), 45663.

47 K. Tashiro, N. Kouno, H. Wang and H. Tsuji, Crystal Structure of Poly(lactic acid) Stereocomplex: Random Packing Model of PDLA and PLLA Chains As Studied by X-ray Diffraction Analysis, *Macromolecules*, 2017, **50**(20), 8048–8065.

48 K. Tashiro, H. Wang, N. Kouno, J. Koshobu and K. Watanabe, Confirmation of the X-ray-Analyzed Heterogeneous Distribution of the PDLA and PLLA Chain Stems in the Crystal Lattice of Poly(lactic acid) Stereocomplex on the Basis of the Vibrational Circular Dichroism IR Spectral Measurement, *Macromolecules*, 2017, **50**(20), 8066–8071.

49 W. Zhou, K. Wang, S. Wang, S. Yuan, W. Chen, T. Konishi and T. Miyoshi, Stoichiometry and Packing Structure of Poly(lactic acid) Stereocomplex as Revealed by Solid-State NMR and 13C Isotope Labeling, *ACS Macro Lett.*, 2018, 7(6), 667–671.

© 2026 The Author(s). Published by the Royal Society of Chemistry

*RSC Appl. Polym.*, 2026, **4**, 651–661 | **661**